Chattering-Free Modelling and Simulation of Power Systems with Inclusion of Filippov Theory

Mohammed Ahsan Adib Murad and Federico Milano
School of Electrical & Electronic Engineering, University College Dublin (UCD), Ireland
mohammed.murad@ucdconnect.ie, federico.milano@ucd.ie

***Abstract*—This paper proposes a general-purpose model of an anti-windup proportional and integral (PI) controller based on Filippov theory and discuss the performance of the proposed PI model for the dynamic analysis of power systems. The proposed model accurately captures non-smooth dynamics according to the IEEE standard 421.5-2016 and effectively removes trajectory deadlock and chattering. The validation of the model is performed considering an automatic voltage regulator and a static synchronous compensator in a single-machine infinite-bus system and the WSCC 9-bus system, respectively.**

***Index Terms*—Anti-windup, chattering, Filippov theory, sliding, hybrid dynamical systems, trajectory deadlock, PI control.**

I. Introduction

Electro-mechanical dynamics of power systems are conveniently modelled through a phasor-based model consisting of a set of continuous nonlinear stiff Differential Algebraic Equations (DAEs). However, large disturbances, controller saturation, generator over-excitation limit and transformer tap changer controllers introduce discontinuities and lead to a formulation of power systems as a set of Hybrid Differential Algebraic Equations (HDAEs), i.e., a set of equations the mix continuous and discrete variables.

In the power system literature, there exists and handful of proposed modelling and implementation methods to HDAEs [1], [2]. However, existing methods cannot handle the *chattering-Zeno*-type deadlock issue, which consists of infinitely many instantaneous switches of the discrete variables. This phenomenon is often observed in anti-windup (AW) proportional and integral (PI) controllers modelled according to the IEEE Std. 421.5-2016 [3], [4], [5]. Until now, only *ad hoc* approaches have been proposed to handle the deadlock issue. For example, a technique based on a dead-band has been proposed in [3]. In this work, we adopt a trajectory continuation based on the mathematical theory developed by Filippov [6].

Filippov theory (FT) generalizes the discontinuities on the first-order ordinary differential equations and provides proper switching conditions. Moreover, if the solution enters into a constrained subset of the state space, typically known as *sliding*, the formalism given by Filippov [6] allows defining a vector field on the sliding surface to properly handle discontinuities. In fact the FT formalism effectively removes the deadlock by smoothing the trajectory is proved in our preliminary results [7].

While effective, the FT-based approach poses several challenges, especially with respect to the numerical integration of DAEs. The main challenge is the definition of the analytical conditions and, thereafter, the implementation of a robust algorithm to automatically switch between different discontinuous states through capturing accurate non smooth dynamics. This paper fills this gap and duly present a general chatter-free model of the IEEE AW PI controller based on FT.

The contribution of this paper is the design of a general-purpose hybrid model of the AW PI controller based on Filippov theory. This approach allows integrating the equations along the deadlock region and removes the chattering and other numerical issues that are shown by existing techniques based on dead-band and semi-implicit formulation presented in [2] and [3].

The remainder of the paper is organized as follows. Section II presents the model of the IEEE model of the AW PI controller and describes the numerical issues that such a model can originate. This section also outlines the techniques proposed in the literature to overcome the numerical issues of the IEEE AW PI model. Section III briefly discusses Filippov theory and Section IV presents the generalized FT based model. Section V presents numerical validations of the proposed model based on the Modelica language [8] as well as on the power system software tool Dome [9]. Finally, Section VI draws conclusions and outlines future work.

II. Formulation

A. IEEE Anti-Windup PI Model

The IEEE Std. 421.5-2016 recommends a conditional integration method to avoid windup effects when the output of the controller exceeds its limits, depicted in Fig. 1. The model consists of the following rules [10]:

$$\begin{aligned} \text{If } y \geq w_{\max} &: w = w_{\max} \text{ and } \dot{x} = 0 \ , \\ \text{If } y \leq w_{\min} &: w = w_{\min} \text{ and } \dot{x} = 0 \ , \\ \text{Otherwise} &: w = y = k_p u + x \text{ and } \dot{x} = k_i u \ , \end{aligned} \tag{1}$$

where u, y, w and x are the input, output without limit, limited output and integrator state variable, respectively; and k_p, k_i, $w_{\max}$ and $w_{\min}$ are the proportional gain, integral gain, maximum and minimum limits, respectively. The state transitions above are illustrated in Fig. 2.

Mohammed Ahsan Adib Murad and Federico Milano are supported by Science Foundation Ireland (SFI) under Grant No. SFI/15/IA/3074.

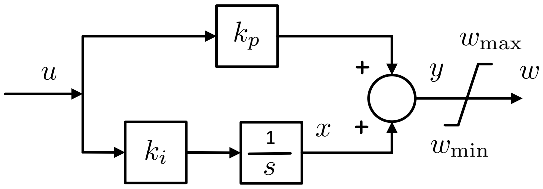

Fig. 1: The anti-windup PI controller block in accordance with the IEEE Std. 421.5-2016 [10].

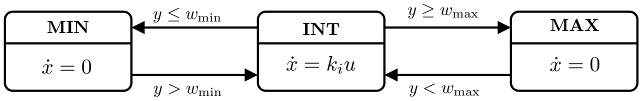

Fig. 2: State transitions of the anti-windup PI controller model.

B. Deadlock

This section describes the numerical issues intrinsic of the IEEE AW PI model. Let us assume that at the beginning of the simulation, the input to the PI controller has an initial integrating state (INT) that is within the controller limits (see Fig. 2) and that such an input the output reaches its maximum limit at t_1. Then, at t_1, one has:

$$x_{t_1} + k_p u_{t_1} = w_{\max} \ , \tag{2}$$

where x_{t_1} and u_{t_1} are the values of the integrator state variable and input, respectively, at t_1. Now, let us assume that the condition to switch back to the INT state are satisfied at t_2, as follows:

$$y < w_{\max} \ . \tag{3}$$

While the state is in the maximum state (MAX), the value x_{t_1} is constant and u_{t_2} in the input at t_2. Thus re-writing (3):

$$x_{t_1} + k_p u_{t_2} < w_{\max} \ \Rightarrow \ u_{t_2} < \frac{w_{\max} - x_{t_1}}{k_p} = u_{t_1} \ , \tag{4}$$

considering $k_p > 0$, if the input u_{t_2} becomes lower than u_{t_1} i.e. condition (4) is full-filled then a transition from the MAX state to the INT state will happen. Assuming at t_2 the input u_{t_2} decreases from u_{t_1} at an integration step and $\Delta u = u_{t_2} - u_{t_1} < 0$. Depending on the integration method, and the step size h, the change in state variable $\Delta x = x_{t_2} - x_{t_1}$, can be obtained as:

- Backward Euler: $\Delta x = h\dot{x}_{t_2} = k_i h u_{t_2}$,
- Forward Euler: $\Delta x = h\dot{x}_{t_{2-1}} = k_i h u_{t_1}$,
- Trapezoidal: $\Delta x = \frac{h}{2}(\dot{x}_{t_{2-1}} + \dot{x}_{t_2}) = k_i \frac{h}{2}(u_{t_1} + u_{t_2})$.

Assuming $k_i > 0$ and $u_{t_2} > 0$, then $\Delta x > 0$. For a feasible transition from the MAX to the INT state at the end of the integration step, $y < w_{\max}$ must hold i.e.

$$\Delta x + k_p \Delta u < 0 \ , \tag{5}$$

using the values of Δx and Δu into (5) for the Backward Euler integration method, one has:

$$\begin{aligned} k_i h u_{t_2} + k_p(u_{t_2} - u_{t_1}) < 0 \ , \\ \Rightarrow \ \frac{u_{t_2}}{u_{t_1}} < \frac{1}{1 + \frac{k_i h}{k_p}} \ . \end{aligned} \tag{6}$$

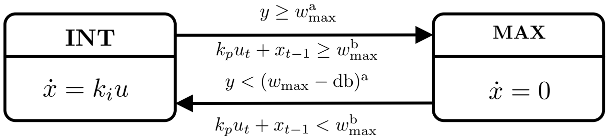
INT
$\dot{x} = k_i u$
$y \geq w_{\max}^{\mathrm{a}}$
$k_p u_t + x_{t-1} \geq w_{\max}^{\mathrm{b}}$
$y < (w_{\max} - \mathrm{db})^{\mathrm{a}}$
$k_p u_t + x_{t-1} < w_{\max}^{\mathrm{b}}$
MAX
$\dot{x} = 0$

Fig. 3: State transitions of the anti-windup PI controller for existing solutions considering: superscripts a and b indicate the deadband- and time delay-based techniques, respectively.

Similarly for the Forward Euler and Trapezoidal method, one has:

$$\frac{u_{t_2}}{u_{t_1}} < 1 - \frac{k_i h}{k_p}, \ \frac{u_{t_2}}{u_{t_1}} < \frac{k_p - \frac{h}{2}k_i}{k_p + \frac{h}{2}k_i} \ . \tag{7}$$

The conditions (6)-(7) need to be satisfied to switch from the MAX to the INT region. Otherwise a deadlock situation arises. The deadlock consists in an infinite loop where the state variables switches between the MAX and INT states. For implicit integration schemes the deadlock also prevents the solver to converge at a given time step and thus the simulation gets stuck. Note that the conditions (6)-(7) depend on the integration step-size h, gain values and current value of the input. It is also important to observe that the deadlock originates due to the time discretization of the numerical integration scheme. For $h \to 0$, in fact, the conditions (6)-(7) are always satisfied and the deadlock does not occur.

It is also important to note that there exist AW implementations other than the IEEE one that do not show numerical issues. These techniques are not considered in this paper as their dynamic behavior is subtly different for large disturbance compared to the IEEE PI model. The interested reader can refer to [11] for a comparison of a variety of AW PI implementations.

C. Existing Solutions

There exists several techniques to avoid the numerical deadlock of the IEEE Std. type AW PI controller. These are the following.

- **Deadband:** This technique is illustrated in Fig. 3 and consists in modifying the state transitions through a deadband [3].
- **Time delay:** To move from the INT state to the MAX or the MIN, this method considers the value of the integrator state variable from the previous time step (see Fig. 3).
- **No-Convergence:** In real-world applications the deadlock eventually disappears because of the variation of the input. A simulator can mimic such a behavior by forcing the solver to move to the next time step after certain number of iterations even if the solver does not converge.
- **Semi-implicit:** This technique consists in using a semi-implicit formulation [12] to convert the integrator state variable into an algebraic variable to continue the simulation during deadlock [2].

The drawbacks of the first three techniques above are that they do not truly represent the hybrid model and introduce artificial chattering. Though it does not show chattering, the semi-implicit formulation does not consider the effect of disturbances of the input to evaluate state transitions while the state is in the deadlock region [4]. Moreover, the semi-implicit formulation requires a solver-dependent implementation and is not supported by most software tool.

III. Filippov Theory

Filippov systems are dynamical systems with discontinuous right-hand side first-order ordinary differential equations (ODEs) [6]. Consider the following switched dynamical system:

$$\dot{x} = f(x) = \begin{cases} f_1(x) & \text{when } h(x) < 0 \\ f_2(x) & \text{when } h(x) > 0 \end{cases} \tag{8}$$

where, the event function $h : \mathbb{R}^n \to \mathbb{R}$ and an initial condition $x(t_0) = x_0$ are known. The state space $\mathbb{R}^n$ is separated by a hyper-surface Σ into two regions R_1 and R_2 as follows,

$$\begin{aligned} R_1 &= \{x \in \mathbb{R}^n \mid h(x) < 0\}, \\ R_2 &= \{x \in \mathbb{R}^n \mid h(x) > 0\}, \\ \Sigma &= \{x \in \mathbb{R}^n \mid h(x) = 0\}, \end{aligned} \tag{9}$$

such that $\mathbb{R}^n = R_1 \cup \Sigma \cup R_2$, assuming at $x \in \Sigma$ the gradient of h never vanishes, i.e. $h_x(x) \neq 0$ for all $x \in \Sigma$.

Filippov convex method [6] states that the vector field on the surface of discontinuity is a convex combination of the two vector fields in the different regions of the state-space:

$$\dot{x} = f(x) = \begin{cases} f_1(x), & x \in R_1 \\ \overline{co}\{f_1(x), f_2(x)\}, & x \in \Sigma \\ f_2(x), & x \in R_2 \end{cases} \tag{10}$$

where, $\overline{co}(f_1, f_2)$ is the minimal closed convex set

$$\overline{co}\{f_1, f_2\} = \{f_F : x \in \mathbb{R}^n \to \mathbb{R}^n : f_F = (1-\alpha)f_1 + \alpha f_2\}, \tag{11}$$

where $\alpha \in [0, 1]$.

Consider the trajectory starting at t_0 with $\dot{x} = f_1(x)$, with $x(t_0) = x_0$ reaches at Σ in finite time (t_k). Then at t_k the trajectory can cross or slide or exit the Σ. In such a situation, the first order theory given by Filippov explains what to do, summarized in the following.

A. Filippov First Order Theory

Filippov first order theory defines the vector field if the solution approaches the discontinuous surface. Let $x \in \Sigma$ and $n(x)$ is the unit normal to Σ at x i.e. $n(x) = \frac{h_x(x)}{\|h_x(x)\|}$ where, $h_x(x) = \nabla h(x)$ and $\nabla = \frac{\partial}{\partial x}$; the components of $f_1(x)$ and $f_2(x)$ onto the normal to the Σ are $n^T(x)f_1(x)$ and $n^T(x)f_2(x)$ respectively.

1) Transversal Crossing: If at $x \in \Sigma$,

$$(n^T(x)f_1(x)).(n^T(x)f_2(x)) > 0, \tag{12}$$

then the trajectory leaves Σ. The system returns to R_1 with $f = f_1$, if $n^T(x)f_1(x) < 0$ or it proceeds to R_2 with $f = f_2$ (see Fig. 4[I]), if $n^T(x)f_1(x) > 0$.

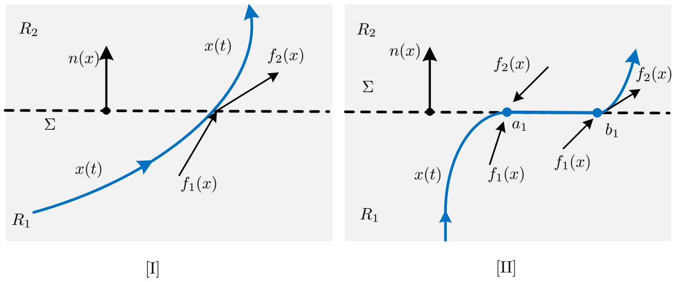

[I]

[II]

Fig. 4: Different regions of the state space with [I] transversal and [II] sliding trajectory.

2) Sliding mode: Sliding occurs, at $x \in \Sigma$, if

$$(n^T(x)f_1(x)).(n^T(x)f_2(x)) < 0 \ . \tag{13}$$

An unique attracting sliding mode occurs if

$$(n^T(x)f_1(x)) > 0 \quad \text{and} \quad (n^T(x)f_2(x)) < 0, \ x \in \Sigma \ , \tag{14}$$

and the solution does not leave Σ (see a_1 in Fig. 4[II]). During sliding, the time derivative f_F is given by:

$$f_F(x) = (1 - \alpha(x))f_1(x) + \alpha(x)f_2(x) \ , \tag{15}$$

where, $\alpha(x)$ is given by [proof, see [6]]:

$$\alpha(x) = \frac{n^T(x)f_1(x)}{(n^T(x)(f_1(x) - f_2(x))} \ . \tag{16}$$

If the signs are opposite in (14) the sliding mode is called *repulsive* and does not generally have a unique solution. For this reason, the repulsive sliding mode is not considered in this work.

3) Exit Conditions: If, while in sliding mode, one of the vector fields drifts away, the solution continues above or below the sliding surface (see b_1 in Fig. 4[II]). The exit point is calculated by finding either the root $\alpha(x) = 0$ or $\alpha(x) = 1$ as appropriate. The following remarks are relevant:

- *If $f_F(x) \neq f_1(x)$, $f_F(x) \neq f_2(x)$ such a solution is often called a sliding motion.*
- If at the point of discontinuity, condition (13) becomes ≤ 0 and $f_1(x) \neq f_2(x)$ then a continuous vector-valued function $f_F(x)$ is given which determines the velocity of motion $\dot{x} = f_F(x)$ along the discontinuity line. If $n^T(x)f_1(x) = 0$ then $f_F(x) = f_1(x)$; if $n^T(x)f_2(x) = 0$ then $f_F(x) = f_2(x)$.

IV. Filippov Based Anti-windup PI Control

FT is based exclusively on ODEs. However, power systems models are described as DAEs. Hence, in power system applications, the input to a PI controller can be an algebraic or a state variable. In this section, we discuss the requirements of a FT-based model of the IEEE Std. AW PI controller and then propose a general design that is compatible with DAEs.

A. General-Purpose Design

Let us consider the PI controller in Fig. 5. This system is represented by (1) and

$$\begin{aligned} \dot{u} &= (v_1 - u)/T \\ v_1 &= v - v^{\mathrm{ref}} \ , \end{aligned} \tag{17}$$

where v_1 is the controlled signal and v^{ref} is the reference signal.

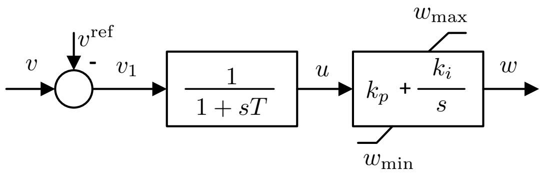

Fig. 5: Generalized IEEE Std. anti-windup PI controller based on FT.

According to FT, the dynamical equations of this system can be represented as (considering the upper limit only),

$$\dot{x} = f(x) = \begin{cases} f_1(x) & \text{if } h(x) < 0 \ , \\ f_2(x) & \text{if } h(x) > 0 \ , \end{cases}$$

with

$$f_1(x) = \begin{pmatrix} (v_1 - u)/T \\ k_i u \end{pmatrix}, \qquad f_2(x) = \begin{pmatrix} (v_1 - u)/T \\ 0 \end{pmatrix},$$

and the surface Σ is defined by zero of $h(x) = y - w_{\max} = k_p u + x - w_{\max}$ and $h_x(x) = [\frac{\partial h(x)}{\partial u} \quad \frac{\partial h(x)}{\partial x}]^T = [k_p \quad 1]^T$.

Let us define $r_1 = h_x^T(x)\, f_1(x)$ and $r_2 = h_x^T(x)\, f_2(x)$ and

$$\begin{aligned} r_1 &= (k_p \ 1) \begin{pmatrix} (v_1 - u)/T \\ k_i u \end{pmatrix} = k_p\big((v_1 - u)/T\big) + k_i u \ , \\ r_2 &= (k_p \ 1) \begin{pmatrix} (v_1 - u)/T \\ 0 \end{pmatrix} = k_p\big((v_1 - u)/T\big) \ . \end{aligned} \tag{18}$$

If a sliding condition is met, the sliding vector field on Σ using (15) and (16) becomes:

$$\begin{aligned} \alpha(x) &= \frac{k_p((v_1 - u)/T) + k_i u}{k_i u} \ , \\ f_F(x) &= \begin{pmatrix} (v_1 - u)/T \\ -k_p((v_1 - u)/T) \end{pmatrix} \ . \end{aligned} \tag{19}$$

An AW PI controller based on (18) and (19) provides correct dynamic response for any disturbance and transient condition. This is obtained through the introduction of the low pass filter. The FT, in fact, requires that all input signals are smooth (i.e. continuous and differentiable) variables. The low pass filter, however introduces a small delay in the transient behaviour of the input and, thus, has to be tuned so that it dynamic is faster than that of the PI controller. Since power system DAE models are intrinsically stiff, the condition on the dynamic of the low pass filter can be easily accommodated by any solver designed for power system analysis.

Based on (18) and (19), the controller has three states, the two states for $h(x) < 0$ (INT) and $h(x) > 0$ (MAX), and a new state called SLIDING, characterized by $h(x) = 0$. For the computer implementation of the FT-based AW PI model, it is convenient to introduce two discrete variables, say z_1 and z_2, into the integrator differential equations, as follows:

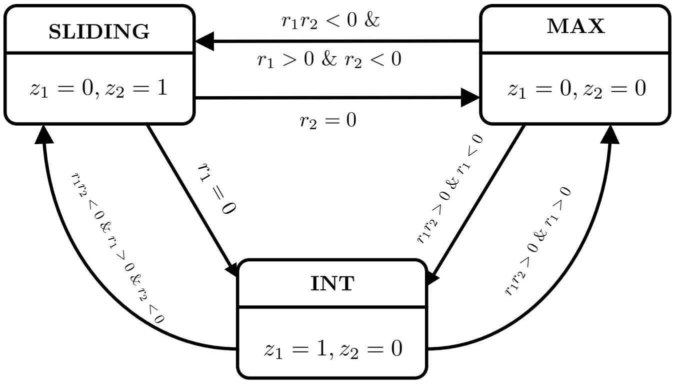

Fig. 6: State transitions of the anti-windup PI controller based on FT (MIN state is not shown).

$$\dot{x} = k_i u \, z_1 - \big(k_p(v_1 - u)/T\big)\, z_2 \ .$$

Fig. 6 shows the change in (z_1, z_2) for the three states and the conditions to move from one state to another. These conditions are based on FT and evaluated the moment at which the event function ($h(x)$) crosses zero. If the solution enters into the sliding region the exit conditions are defined based on (19). In particular, $\alpha(x) = 0$ and $\alpha(x) = 1$ are the conditions that indicate to move to the INT and MAX regions, respectively.

Following a similar procedure a complete state transition scheme can be obtained to consider the lower limit i.e. the MIN state.

V. Case Study

This section discusses the software implementation of the proposed FT-based implementation of the AW PI and validates such a model through time domain simulations. Two applications are considered: (i) an excitation system in a Single Machine Infinite Bus (SMIB) system; and (ii) a Static Synchronous Compensator (STATCOM) in WSCC 9-bus test system.

A. Software Implementation

The generalized design of the AW PI controller can be implemented in a computer language considering an *event driven* or a *time stepping* approaches [13]. The former method simulates the system with accurately detecting the actual event time [14] and the latter method without [2]. The case study of the SMIB system considers an *event driven* implementation utilizing the Modelica language [8] and the WSCC-9 bus systems considers a *time stepping* implementation utilizing the Python-based power system software tool Dome [9].

The deadband (DB) and time delay (TD) based PI controllers described in Section II-C are also implemented for comparison. In all case studies the value of DB is 0.001. The

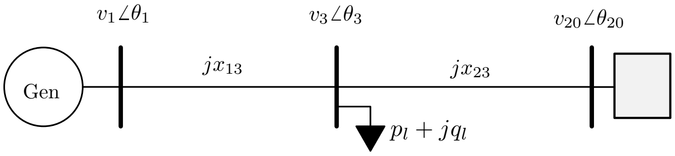

Fig. 7: Single-machine infinite-bus test system.

TABLE I: Parameters of the SMIB system

Name	Values
Generator	$M = 8$, $D = 0$, $x'_d = 0.25$, $x_d = 1$, $p_m = 1$, $T'_{d0} = 6$
Line	$x_{13} = 0.3$, $x_{23} = 0.5$
Load	$p_{l0} = 0.7$, $q_{l0} = 0.01$
AVR	$T_r = 0.005$, $k_{pr} = 10$, $k_{ir} = 25$, $k_{pm} = 2$, $k_{im} = 20$, $T_a = 0.02$, $T_g = 0.005$, $k_g = 0.18$, $v_{\rm G}^{\rm max} = 99$, $v^{\rm ref} = 1$
PSS	$k_s = 1.5$, $T_1 = 0.23$, $T_2 = 0.12$

time constant of the lag filter is $T = 0.0001$ s for the FT-based AW PI model.

B. SMIB with an ST4C type Excitation System

Fig. 7 shows the SMIB system considered in this example. The generator is equipped with an Automatic Voltage Regulator (AVR) and a Power System Stabilizer (PSS) as depicted in Fig. 8. The generator model is a third order type; the PSS consists of a stabilizer gain and a lead lag block [15]. The AVR is a simplified version of the ST4C static excitation system [10].

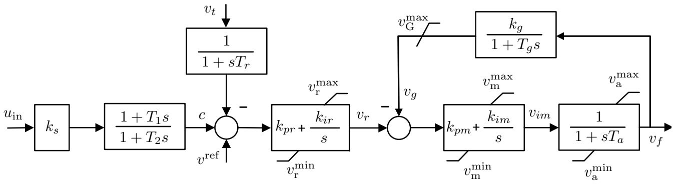

Fig. 8: Control diagram of the ST4C static excitation system with inclusion of a PSS.

The input to the PSS is the rotor speed of the generator and the active and reactive power of the load are modelled as $p_l = p_{l0}(\frac{v_3}{v_{30}})$, $q_l = q_{l0}(\frac{v_3}{v_{30}})^2$, where v_{30} is the initial voltage from power flow calculation. The parameters of all components of the SMIB system are given in Table I. For all PI models and the lag filter model (see Fig. 8), the maximum and minimum values of the AW limiter are 2 and -0.8, respectively.

As discussed in Section II-B, the numerical integration of the IEEE AW PI controller can fail as a consequence of several factors. In the following, we consider two disturbances for which the solver gets stuck for validating the FT based AW PI controller. The Modelica-based simulation tool Dymola [16] is used to solve all simulations for this case study.

1) Contigency I: A three phase fault occurring at 5 s and cleared after 100 ms is simulated in the SMIB system. Following the disturbance, both the PI controllers and the lag block of the AVR reaches their limits. Fig. 9 shows the state-space representation $(x_{im}, \dot{x}_{im})$ of one the AW PI controller included in the AVR (see Fig. 8).

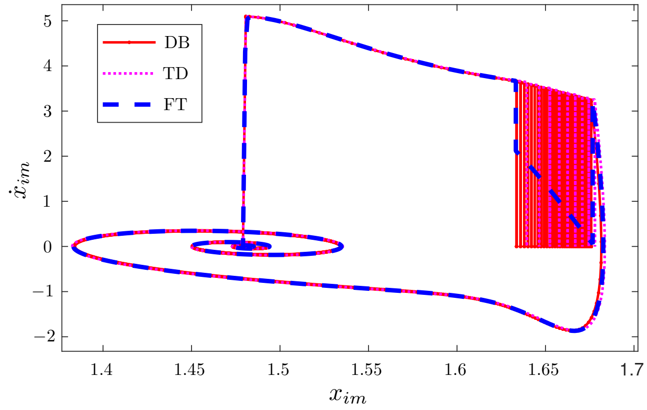

Fig. 9: Time derivative of the integrator state variable ($\dot{x}_{im}$) with respect to the integrator state variable (x_{im}).

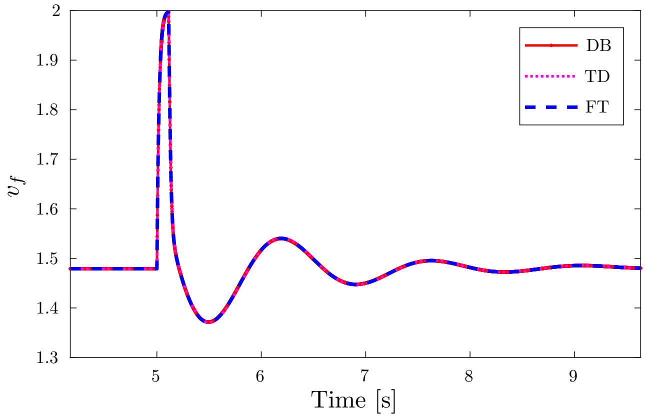

Fig. 10: Trajectory of the output of the AVR.

The FT-based AW PI controller provides a smooth response compared to the DB and TD implementations. Thus the main advantage of the FT model is that it removes the artificial chattering. To realize how this chattering is removed observe the sliding vector field in (19). During the sliding mode, the FT-based implementation allows increasing the integrator state variable consistently to the decrease of proportional channel of the controller. On the other hand, DB and TD models increase the integrator state variable by imposing some delay. This delay originates the chattering. Compared to these techniques, the FT-based AW PI model requires less state events and is thus less computationally demanding along the chattering region.

For completeness, Fig. 10 illustrates the output of the AVR, i.e. the field voltage (v_f) and the response is identical for all the methods.

2) Contigency II: The SMIB system is simulated by increasing the voltage reference set-point ($v^{\rm ref} = 1.03$ pu) and the load ($p_{l0} = 0.8$ pu, $q_{l0} = 0.02$ pu) at $t = 5$ s. Fig. 11 shows the time derivative of integrator state variable ($\dot{x}_{im}$) with respect to time. Following the disturbance, the integrator

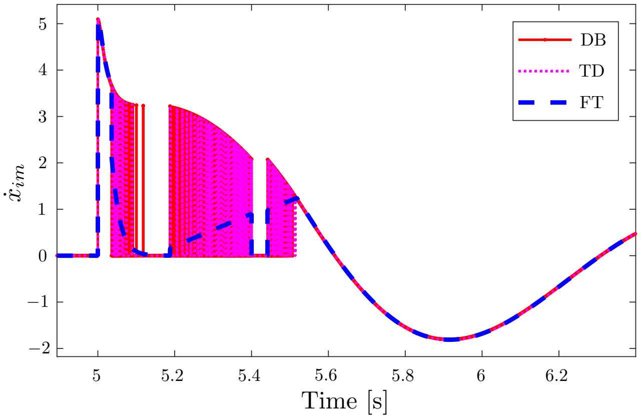

Fig. 11: Response of the time derivative of integrator state variable ($\dot{x}_{im}$) with respect to time.

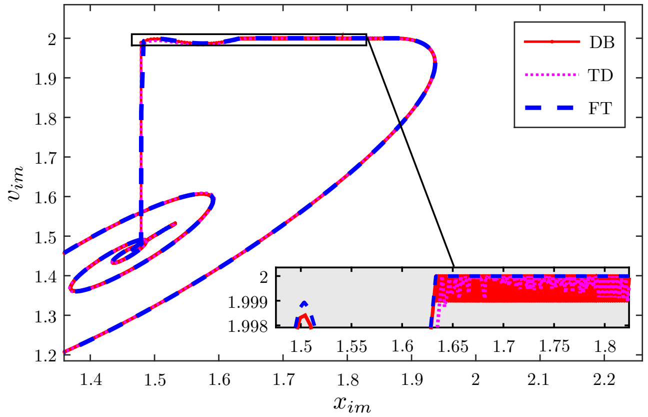

Fig. 12: Response of the output (v_{im}) with respect to the integrator state variable (x_{im}).

state variable x_{im} enters into the deadlock region for the DB and TD models. Then, x_{im} into the MAX state, comes back to the deadlock region and chatters again. While chattering, another step increase in the load ($p_{l0} = 0.82$ pu, $q_{l0} = 0.025$ pu) is applied at $t = 5.4$ s which drives x_{im} to the MAX state exactly at 5.4 s.

Except for the chattering, the FT model shows same trajectory for x_{im} as the DB and TD models between the SLIDING and MAX states while the solution is at the SLIDING state for a step increase in the reference set-point. Thus the FT based method provides accurate dynamic response considering all kinds of disturbance. This proves that the proposed model is consistent with existing implementation and captures accurate hybrid system dynamics without any chattering.

Fig. 12 shows the output (v_{im}) of the AW PI controller included in the AVR with respect to the integrator state variable (x_{im}). The trajectory obtained with the DB and TD models continues through switching during the deadlock period. Note that the number of switches depends on the deadband width/delay magnitude as well as the time step of the simulation. The latter dependency indicates that the chattering actually a numerical issue, not a physical behaviour of the controller. On the other hand, the FT-based implementation is independent from the time step, as long as the time step is compatible with the numerical stability of the integration method and adequate for the DAE stiffness.

C. VSC-based STATCOM

This case study considers a VSC (Voltage-Sourced Converter)-based STATCOM in the WSCC 9-bus test system. The STATCOM is a shunt Flexible AC Transmission System (FACTS) device utilized to regulate the voltage of the bus at which it is connected. To model the STATCOM an Average Value Model (AVM) of the converter and a vector-current control based on dq-composition with grid voltage as phase reference is used [17]. The converter and its control loops are shown in Fig. 13. The d and q components in the outer control are utilized to control AC and DC voltages respectively and the inner loop controls the decoupled d and q currents. Both outer and inner level controllers are AW PI controllers.

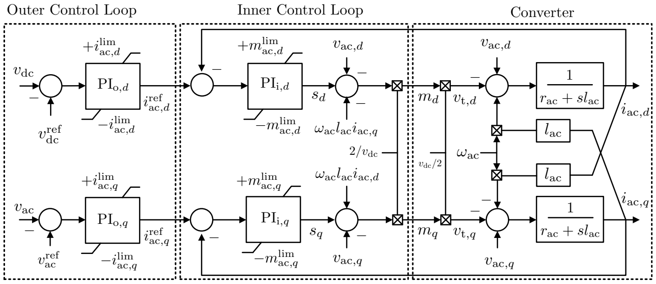
Outer Control Loop
Inner Control Loop
Converter
v_{dc}
$v_{\mathrm{dc}}^{\mathrm{ref}}$
$+i_{\mathrm{ac},d}^{\mathrm{lim}}$
$\mathrm{PI}_{\mathrm{o},d}$
$-i_{\mathrm{ac},d}^{\mathrm{lim}}$
$i_{\mathrm{ac},d}^{\mathrm{ref}}$
$+m_{\mathrm{ac},d}^{\mathrm{lim}}$
$\mathrm{PI}_{\mathrm{i},d}$
$-m_{\mathrm{ac},d}^{\mathrm{lim}}$
s_d
$v_{\mathrm{ac},d}$
$\omega_{\mathrm{ac}} l_{\mathrm{ac}} i_{\mathrm{ac},q}$
$2/v_{\mathrm{dc}}$
m_d
$v_{\mathrm{t},d}$
$v_{\mathrm{dc}}/2$
ω_{ac}
l_{ac}
$\frac{1}{r_{\mathrm{ac}} + s l_{\mathrm{ac}}}$
$i_{\mathrm{ac},d}$
$i_{\mathrm{ac},q}$
v_{ac}
$v_{\mathrm{ac}}^{\mathrm{ref}}$
$+i_{\mathrm{ac},q}^{\mathrm{lim}}$
$\mathrm{PI}_{\mathrm{o},q}$
$-i_{\mathrm{ac},q}^{\mathrm{lim}}$
$i_{\mathrm{ac},q}^{\mathrm{ref}}$
$+m_{\mathrm{ac},q}^{\mathrm{lim}}$
$\mathrm{PI}_{\mathrm{i},q}$
$-m_{\mathrm{ac},q}^{\mathrm{lim}}$
s_q
$\omega_{\mathrm{ac}} l_{\mathrm{ac}} i_{\mathrm{ac},d}$
$v_{\mathrm{ac},q}$
m_q
$v_{\mathrm{t},q}$
−

Fig. 13: VSC converter with its inner and outer control in dq-frame.

TABLE II: VSC-based STATCOM parameters.

Name	Values
Converter	$l_{\mathrm{ac}} = 0.401$ pu, $r_{\mathrm{ac}} = 0.003$ pu
Current Limits	$i_{\mathrm{ac},q}^{\mathrm{lim}} = \pm 0.3$ pu, $i_{\mathrm{ac},d}^{\mathrm{lim}} = \pm 0.01$ pu
Outer Control	$k_p^{\mathrm{o},q} = 5.5$, $k_p^{\mathrm{o},d} = 50$, $k_i^{\mathrm{o},q} = 45$, $k_i^{\mathrm{o},d} = 25$
Inner Control	$k_p^{\mathrm{i},q} = 0.2$, $k_p^{\mathrm{i},d} = 0.2$, $k_i^{\mathrm{i},q} = 20$, $k_i^{\mathrm{i},d} = 20$

The test network consists of three synchronous machines, three two-winding transformers, three loads and six transmission lines. All generators are equipped with AVRs and Turbine Governors (TGs). The dynamic data of this test network is provided in [18]. The VSC-based STATCOM is connected at bus 8 and the parameters are given in Table II. The STATCOM without any storage can only provide reactive power support except for some losses. Therefore current limits in the outer loops are set by prioritizing the q-axis component [11]. The simulations of this example have been solved with DOME [9].

1) Contingency: A three phase fault occurring at $t = 1$ s is applied for 60 ms and cleared through disconnecting the line in between buses 6 and 9. The line is reconnected at $t = 6$ s. The dynamic response of the q-axis current reference ($i_{\mathrm{ac},q}^{\mathrm{ref}}$) is shown in Fig. 14 for DB and FT models. The TD model is not compared in this case study as it shows similar results as

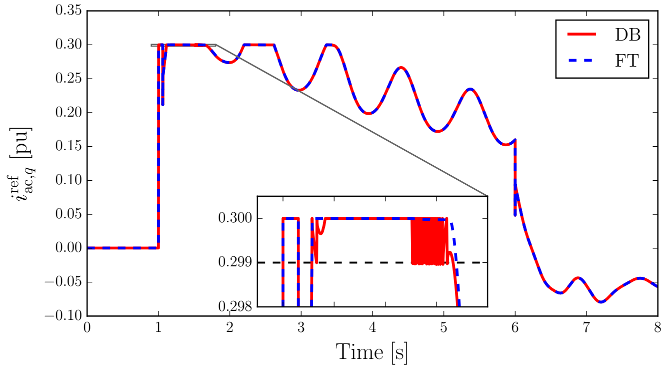

Fig. 14: Response of the output of the AC voltage controller in the outer loop.

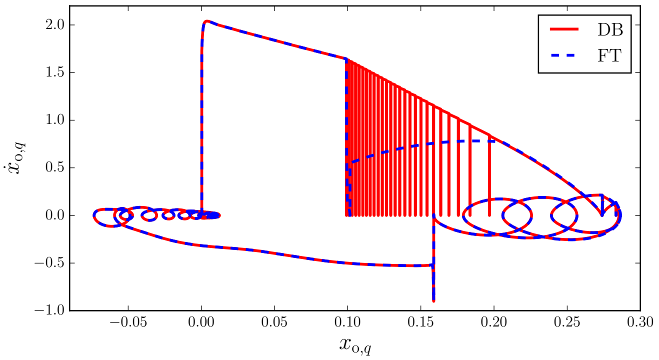

Fig. 15: Time derivative of the integrator state variable with respect to the state variable of the AC voltage controller in the outer loop.

the DB one.

Before the occurrence of the fault, the STATCOM does not provide any reactive power so the $i^{\mathrm{ref}}_{\mathrm{ac},q}$ is zero until $t = 1$ s. However following the fault, the $i^{\mathrm{ref}}_{\mathrm{ac},q}$ reaches its limit in the attempt to regulate the voltage and comes back within the limit when the fault is cleared. Then the controller shows an oscillatory response to reach a steady state solution. The AW PI controller enters into a deadlock region in two occasions (zoomed in Fig. 14). In the deadlock region the controller based on the DB model shows numerous chattering whereas the FT-based controller shows a smooth response. The trajectories of the time derivative of the integrator state variable of the AW PI controller of the AC voltage controller based on DB and FT models are shown in Fig. 15, confirming the ability of the FT implementation to avoid chattering.

This example also confirms the versatility of the proposed FT approach, which proves to be suitable for both event-driven (Dymola) and time-stepping (DOME) software tools.

VI. Conclusions

A general-purpose state transition diagram is proposed to model and implement the IEEE Std. 421.5-2016 AW PI controller to remove trajectory deadlock and chattering based on the FT. The conditions to automatically switch to different discontinuous vector fields are also duly derived. The case studies show that the proposed design provide accurate dynamic response and is suitable for implementation in a power system software tool.

Future work will extend the FT-based AW PI controller to impose time varying limits.

References

[1] I. A. Hiskens and P. J. Sokolowski, "Systematic modeling and symbolically assisted simulation of power systems," *IEEE Transactions on Power Systems*, vol. 16, no. 2, pp. 229–234, May 2001.

[2] D. Fabozzi, A. S. Chieh, P. Panciatici, and T. Van Cutsem, "On simplified handling of state events in time-domain simulation," *Proceedings of the 17th PSCC*, 2011.

[3] I. A. Hiskens, "Dynamics of type-3 wind turbine generator models," *IEEE Transactions on Power Systems*, vol. 27, no. 1, pp. 465–474, Feb 2012.

[4] D. Fabozzi, S. Weigel, B. Weise, and F. Villella, "Semi-implicit formulation of proportional-integral controller block with non-windup limiter according to IEEE Standard 421.5-2016," in *Bulk Power Systems Dynamics and Control Symposium (IREP)*, 2017, pp. 1–7.

[5] I. A. Hiskens, "Trajectory deadlock in power system models," in *2011 IEEE International Symposium of Circuits and Systems (ISCAS)*, May 2011, pp. 2721–2724.

[6] A. F. Filippov, *Differential Equations with Discontinuous Righthand Sides*. Kluwer Academic Publishers, 1988.

[7] M. A. A. Murad, B. Hayes, and F. Milano, "Application of filippov theory to the IEEE Standard 421.5-2016 anti-windup PI controller," in *2019 IEEE Milan PowerTech*, June 2019, pp. 1–6.

[8] The Modelica Association. [Online]. Available: https://modelica.org

[9] F. Milano, "A Python-based software tool for power system analysis," in *IEEE PES General Meeting*, Vancouver, BC, 2013, pp. 1–5.

[10] "IEEE recommended practice for excitation system models for power system stability studies," *IEEE Std 421.5-2016 (Revision of IEEE Std 421.5-2005)*, pp. 1–207, Aug 2016.

[11] M. A. A. Murad and F. Milano, "Modeling and simulation of PI-controllers limiters for the dynamic analysis of VSC-based devices," *IEEE Transactions on Power Systems*, vol. 34, no. 5, pp. 3921–3930, Sep. 2019.

[12] F. Milano, "Semi-implicit formulation of differential-algebraic equations for transient stability analysis," *IEEE Transactions on Power Systems*, vol. 31, no. 6, pp. 4534–4543, Nov 2016.

[13] L. Dieci and L. Lopez, "A survey of numerical methods for IVPs of ODEs with discontinuous right-hand side," *Journal of Computational and Applied Mathematics*, vol. 236, no. 16, pp. 3967 – 3991, 2012.

[14] P. T. Piiroinen and Y. A. Kuznetsov, "An event-driven method to simulate Filippov systems with accurate computing of sliding motions," *ACM Trans. Math. Softw.*, vol. 34, no. 3, pp. 13:1–13:24, May 2008.

[15] F. Milano, *Power System Modelling and Scripting*, ser. Power Systems. Springer Berlin Heidelberg, 2010.

[16] Dymola: Dynamic Modeling Laboratory. [Online]. Available: https://www.3ds.com/

[17] Y. Amirnaser and I. Reza, *Voltage-sourced converters in power systems: modeling, control, and applications*. IEEE Press, 2012.

[18] P. M. Anderson and A. A. Fouad, *Power system control and stability*. John Wiley & Sons, 2008.